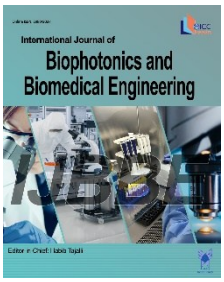

Volume 5, Issue 2, (2025) Article 10

International Journal of

Biophotonics and Biomedical Engineering (IJBBE)

https://doi.org/10.57647/ijbbe.2025.0502.10

A Plasmonic Optical Waveguide Based on the Surface Plasmon Polariton of Graphene Nanoribbon Coupled with Graphene Quantum Dot Scattering Effect for Biosensor Applications

Mahmoud Baghbanzadeh[1], Hassan Rasooli Saghai[2,*], Hamed Alipour-Banaei[3], Shahram Mojtahedzadeh[1], Mohammad Ali Tavakoli Ghazi Jahani[1]

[1] *Department of Electrical Engineering, Aza.C., Islamic Azad University, Azarshahr, Iran*
[2] *Department of Electrical Engineering, Ta.C., Islamic Azad University, Tabriz, Iran*
[3] *Department of Electronics, Ta.C., Islamic Azad University, Tabriz, Iran*

***Corresponding author:** h-rasooli@iau.ac.ir

Original Research

Received:
21 September 2025

Revised:
12 October 2025

Accepted:
21 October 2025

Published in Issue:
31 December 2025

Abstract

We introduce a plasmonic waveguide that consists of three layers, including a nonlinear graphene nanoribbon (GNR), a stack of 6 layers of dielectric-like graphene, and a Si layer. We compute the permittivity of the GNR based on Kubo formalism, considering the third-order nonlinear response of the graphene medium. The thickness, width, and Fermi level of GNR are considered to be 0.34 nm, 50 nm, and 2.4 eV, respectively. Excitation of surface plasmon resonance (SPR) in combination with the Kerr effect establishes a broad resonance mode. Then we embed an array of graphene quantum dots (GQDs) with a diameter of 66 nm between GNRs. The permittivity of GQD is computed through the Cole-Cole model. The scattering effect of GQDs supports the establishment of a narrow resonance mode. Coupling between the broad and narrow resonances results in a Fano resonance in the wavelength of 1100 nm, which is highly sensitive to any change in the refractive index of the surrounding medium. So we design a biosensor based on our waveguide, where a 10 nm air gap is introduced between two parts of the biosensor. Replacing the air gap with a biomaterial medium shifts the Fano resonance position. This feature can be used to detect neurodegenerative disorders. The sensitivity and FOM of the proposed biosensor are computed as 471 nm/RIU and 43, respectively.

Keywords: Biosensor; Kerr nonlinearity; Scattering effect; Surface plasmon polariton; Waveguide

Cite this article: Baghbanzadeh, M., Rasooli Saghai, H., Alipour-Banaei, H., Mojtahedzadeh, Sh., Tavakkoli Ghazi Jahani, M. A., A Plasmonic Optical Waveguide Based on the Surface Plasmon Polariton of Graphene Nanoribbon Coupled with Graphene Quantum Dot Scattering Effect for Biosensor Applications, *Int. J. Biophoton. Biomed. Eng.*, 5(2) Article 10 (2025). doi.org/10.57647/ijbbe.2025.0502.10

1. Introduction

Surface plasmon resonance (SPR) biosensors are optical sensors that use surface plasmon polariton (SPP) waves to probe the interactions between biomolecules and the sensor surface. These sensors have attracted great attention due to their high sensitivity, reliability, label-free, and ability to perform real-time detection [1]. SPP

is the non-radiation mechanism of plasmonic effect that arises at the interface of metal/dielectric due to the interaction of electromagnetic waves propagating along the interface and free electrons of the metallic nanostructure. The coupling of an electromagnetic wave with the collective excitation of free metallic electrons results in polarization of electrical charges. This polarization establishes an electric field that is highly confined by a dielectric material.

SPP causes the evanescent electromagnetic waves to be emitted perpendicular to the confined electrical field and decay into the interface [2-4]. SPP-based structures coupled with a narrow resonance have a high sensitivity to changes in the surrounding refractive index (RI). This feature plays a key role in exploiting the SPP effect on the design of biosensors. In addition, SPP biosensors benefit from miniaturized size, rapid response times, and improved light-matter interaction [5].

One of the most significant devices for the excitation of SPP for biosensor applications is plasmonic waveguides. The plasmonic waveguides enable low-loss light propagation and are thereby used to connect components and devices. These devices confine and guide light through a sub-wavelength scale enabling device dimensions to be shrunk to those of electronic circuits [6, 7]. Conventionally, plasmonic waveguide-based biosensors are designed based on a metal/dielectric structure with silver, gold, Al, and TiN as metallic members. The Ag/insulator/Ag waveguide at the wavelength range of 1000~1500 nm [8], the Ag/SiO2 waveguide at the wavelength range of 600~1400 nm [9], and the Au-based waveguide biosensor at the wavelength range of 1500~1700 nm [10] are examples of this kind of waveguides. Where silver is oxidized when exposed to air, performance is reduced, and life is shortened. Biomolecules show poor adsorption on gold, limiting sensitivity. The spectral broadening caused by interband transitions also obstructs the performance of the sensor. In addition, the weak biocompatibility of the gold and silver membranes may cause cell rejection and produce false signals [11]. Introduction of graphene, a 2D hexagonal lattice of carbon atoms and a tunable nanomaterial, has opened new approaches to this field. Due to extraordinary optical properties, graphene SPP has been considered as an alternative candidate to replace the metal-based plasmonic devices and has attracted great attention in the plasmonic field. Graphene exhibits a relatively large conductivity, high carrier mobility, long optical relaxation times, and could potentially provide a large plasmon wave propagation distance. It is well established that graphene SPP can provide strong optical confinement and have extreme field confinement with volumes of~106 times smaller than the diffraction limit. More importantly, the graphene SPP effect can be tuned via its Fermi level, which can be adjusted by means of chemical doping and gate voltage. Besides its electrical and optical confinement and tunable SPP effect, the outstanding features of graphene nanostructures, such as graphene nanoribbon (GNRs), are under the influence of their high edge/bulk ratio. Last but not least, when the imaginary part of the graphene's complex conductivity is positive, a graphene layer behaves like a thin metal film that supports transverse-magnetic (TM) surface waves. Although an experimental result shows that a graphene polarizer can support TE-mode surface wave propagation [2, 4, 12, 13].

In this study, we propose a resonator/dielectric structure in which a nonlinear GNR array performs as a resonator on the surface of a stack of dielectric-like graphene. Excitation of SPP enhances the medium nonlinearity, in which a change in the RI of the surrounding medium modifies the reflectance characteristic. Considering the Kerr effect, we compute the permittivity of GNR based on the Kubo-Drude formalism. While this structure provides a broad resonance, we locate an array of GQD between GNRs to produce a narrow resonance utilizing the scattering effect of GQDs. The coupling between the broad resonance and the narrow resonance modes establishes a Fano resonance in the reflectance profile that is ideal for bio-sensing applications.

2. Literature Review

Wu presented an SPR-based graphene biosensor by coating graphene over a gold film. Compared with a conventional SPR biosensor, the use of the graphene not only improves the adsorption efficiency of biomolecules, but also detects the change in refractive index near the surface of the sensor by using an attenuated total reflection (ATR) method [14, 15]. Salihoglu et al. fabricated an SPR graphene sensor integrated with a microfluidic device to study nonspecific physical interaction between the graphene layer and proteins. They anticipated that graphene-based SPR can be used to analyze the adsorption of organic solutes from an aqueous solution on a graphitic surface, which has a wide spectrum of applications for environmental protection and the pharmaceutical industry [16]. Ruan et al. coupled graphene SPR in a waveguide to realize an ultrasensitive terahertz biosensor with the highest sensitivities. Their result is two orders of a conventional SPR sensor. Furthermore, they found that when a sensing medium is in the vicinity of water in THz, the sensitivity increases with increasing RI of a sensing medium [17]. Salehnezhad et al. designed a sensitive biosensor based on the graphene

SPR effect with the structure of graphene-MsO_2 for the detection of biomolecules. The detection range for the proposed structure with the size of 1112 nm x 2000 nm is obtained with a RI of 0.005 [18]. Dai et al. proposed a biosensor constructed by periodic GNRs hybridized on a distributed planar waveguide. In this structure, the periodic GNRs can not only excite the graphene SPP, but can also work as a grating to provide the momentum-matching condition for exciting the waveguide mode. This structure can be applied as a self-referenced RI sensor [19].

Excitation of SPP in the graphene is the main interest of this research to design a graphene-based SPR biosensor, where it is well established that graphene SPP can provide strong optical confinement [20, 21]. In addition, graphene is a strongly nonlinear material. Its remarkable third-order nonlinear optical response and related large nonlinear susceptibility have been put forward both in theories and experiments. This nonlinearity results in strong field conditions and improvement of electromagnetic waves emitting [12, 22]. Related to this category, some research has been conducted to design nonlinear plasmonic waveguides. Jiang et al. sandwiched a dielectric between two graphene layers to design a graphene plasmonic waveguide. They analyzed the influence of field intensity and chemical potential on the dispersion relation, and found that the nonlinearity of graphene strongly affects the dispersion relation [22]. Xiao Yong and Rui LI did a comparison between TM and TE SPP for air/graphene/silica/silicon structure. This waveguide consists of a graphene layer located on the silica/silicon layers. The authors derived the dispersion relations for TM and TE SPPs by starting from Maxwell's equations and applying boundary conditions. It was concluded that TM mode is a bound mode, while the TE mode is a lossy mode, and the effective index of the graphene-supported TM mode increases as the operation frequency increases. The authors deduce that TM mode has better confinement than conventional metal-based structures [23].

3. Material and Method

Optical nonlinearity is an anharmonicity of electronic motion in a strong electromagnetic field that results in mixing of the incident lights and the production of new fields. These lights and fields oscillate at the sums and differences of the incident frequencies and can propagate in various directions. Optical mixing can be classified into two categories: second-order mixing and third-order mixing. The third-order response is known as the optical Kerr effect and results in nonlinear modifications of the RI. The Kerr effect is a phenomenon in which two or more monochromatic strong lights of different frequencies are incident on a nonlinear medium, such as a plasmonic structure [24, 25]. In this study, we consider the graphene layer to be a nonlinear medium with plasmonic behavior. We model the graphene layer based on its surface conductivity through Equ 1.

$$\sigma_G(\omega) = \sigma_L(\omega) + \sigma_{NL}(\omega) \tag{1}$$

where σ_G is the total conductivity of the graphene, ω is the angular frequency of the incident light, σ_L and σ_{NL} are the linear and nonlinear conductivities of the graphene, respectively [22]. σ_L should express the plasmonic behavior of the graphene layer. The outstanding feature of the graphene in the plasmonic state can be configured based on its Fermi level and relaxation time. These parameters are adjustable through the Kubo model. So, we compute the σ_L applying the Kubo formalism through Eq. 2.

$$\begin{aligned}\sigma_L(\omega) &= \frac{i2e^2k_BT}{\pi\hbar^2(\omega + i\tau_G^{-1})}\ln\left[2\cosh\left(\frac{E_f}{2k_BT}\right)\right] \\ &+ \frac{e^2}{4\hbar}\left[\frac{1}{2} + \frac{1}{\pi}\arctan\left(\frac{\hbar\omega - 2E_f}{2k_BT}\right)\right. \\ &\left. - \frac{i}{2\pi}ln\frac{\left(\hbar\omega + 2E_f\right)^2}{\left(\hbar\omega - 2E_f\right)^2 + 4k_B^2T^2}\right]\end{aligned} \tag{2}$$

where e is the electron charge, K_B and $\hbar$ are Boltzmann and reduced Planck constant respectively, T is the simulation temperature, and equals 300°k, τ_G is the carrier relaxation time in the graphene layer, and E_f is the Fermi energy level of the intrinsic graphene layer [3, 26-28]. The Drude model is utilized to calculate τ_G. The modified Drude model for massless Dirac electrons in graphene layer is presented in Eq. 3.

$$\tau_G = \frac{\mu E_f}{ev_f^2} \tag{3}$$

where μ is the graphene mobility, and equals 10000 $cm^2/V.s$, v_f is the carrier Fermi velocity and, equals $0.95 \times 10^8\ cm/s$ [29, 30]. The Kubo model contains both intraband and interband conductivity terms. For $2E_f < \hbar\omega$, the interband transition is dominated, which covers the high frequency band from the infrared to the visible band, and for $2E_f > \hbar\omega$, the intraband transition is dominated, which covers the low frequency band, such as THz bands [31]. The nonlinear response of the graphene is proportional to the reciprocal of the third-order response (σ_3) and the square of the electric field

amplitude (E) of the incident light. It means that a giant nonlinear response of the graphene will be triggered under the conditions of a low signal frequency and a high pump power density. From the abovementioned explanation, it can be understood that σ_{NL} is computed through [12, 22]:

$$\sigma_{NL}(w) = \sigma_3(w)|E|^2 \quad (4)$$

$$\sigma_3(w) = -i\frac{9}{8}\frac{e^2}{\pi\hbar^2}\frac{(ev_f)^2}{E_f\omega^3} \quad (5)$$

We consider the self-phase modulation of the optical Kerr effect to be the dominant nonlinear response in the graphene sheet. Because it has been proven that the cross-phase modulation has a very slight contribution to the nonlinearity response [12].

A uniaxial anisotropic meta-material is identified by the permittivity tensor. While the graphene layer with a thickness of much less than the wavelength range is a sub-wavelength meta-material that, based on effective-medium theory, can be considered to have an isotropic permittivity. The homogeneous permittivity of the graphene layer is obtained through Eq. 6

$$\varepsilon_{eq-G} = \frac{1}{3}\varepsilon_{\perp} + \frac{2}{3}\varepsilon_{\parallel} \quad (6)$$

where ε_{eq-G} is the homogeneous permittivity of the graphene layer, $\varepsilon_{\perp}$ and $\varepsilon_{\parallel}$ are the out-of-plane and the in-plane permittivities of the graphene layer. $\varepsilon_{\perp}$ is obtained 2.5 from the dielectric constant of graphite [32]. $\varepsilon_{\parallel}$ is calculated through Eq. 7.

$$\varepsilon_{\parallel}(\omega) = \varepsilon_{\perp} + \frac{i\sigma_G(\omega)}{\omega\varepsilon_0 T_G} \quad (7)$$

where is the vacuum dielectric constant, and equals 1, and T_G is the thickness of the graphene layer [2]. The $\varepsilon_{\perp}$ is dominated by the dielectric constant of graphite and does not show any comsiderable change versus wavelength. Figure 1 demonstrates the imaginary part of the nonlinear graphene layer as a function of wavelength.

Our design strategy is based on a medium that consists of a plasmonic nonlinear graphene nanoribbon and a dielectric-like graphene substrate. So, we must model a graphene layer that has dielectric behavior. It has proven that the modeling of the graphene permittivity with Eq.8 results in a dielectric-like behavior in the graphene layer [33].

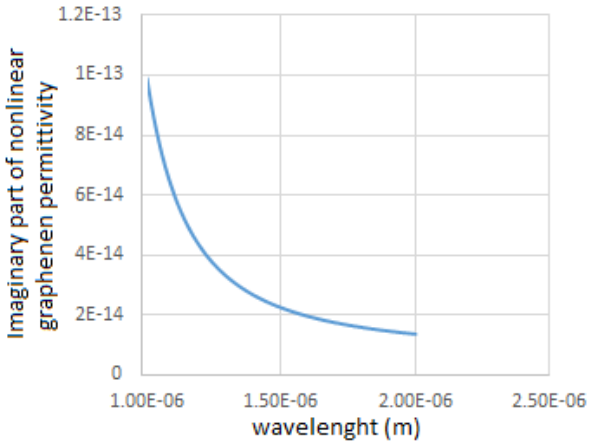

Figure 1. Imaginary part of nonlinear graphene permittivity as a function of wavelenght

$$\varepsilon_{di-G} = \varepsilon_{\infty} - \frac{\omega_{gra}^2}{\omega^2 + i\omega\gamma_{gra}} + \sum_{j=1}^{m}\frac{\Delta\varepsilon_j\Omega_j^2}{\Omega_j^2 - \omega^2 - i\omega\Gamma_j} \quad (8)$$

where m = 3, ε_{∞} = 1.964, $\Delta\varepsilon_j$ = (6.99, 1.69, 1.53), $\hbar\Gamma_j$ = (7.99, 2.01, 0.88) eV, $\hbar\omega_{gra}$ = 6.02eV, $\hbar\gamma_{gra}$ = 4.52 eV, $\hbar\Omega_j$ = (3.14, 4.03, 4.59) eV [33].

Figure 2 demonstrates the structure of the proposed plasmonic nonlinear waveguide. This waveguide consists of three layers including, a plasmonic nonlinear graphene nanoribbon (PNGN), a stack of the multi-layer dielectric-like graphene (MDG), and a silicon (Si) layer. Si is the main block of the majority of the electronic and optical devices due to its great abundance and the well-developed process [34]. The thickness of PNGN is set to be 0.34 nm as the graphene layers are separated by a thickness of 0.34 nm in graphite [35], and its width is chosen as 50 nm. PNGN layers are arranged with a distance of 150 nm from each other. In electronic engineering literature, the Fermi level of the graphene layer has been considered to be 0.3~2.4 eV [36]. By increasing the Fermi level from 0.3 eV, the graphene layer behavior changes from a dielectric with high loss to a metal without loss [37]. Also, by increasing the Fermi level, the plasmonic resonance effect of graphene nanoribbon is intensified [38]. So, in numerical solution, we set $E_f = 2.4\ eV$. There are some reports, that have considered the thickness of graphene layer as 0.5 nm, 0.8 nm, and 1 nm [3, 27, 39]. In this design, we consider the thickness of the dielectric-like graphene layer to be 1 nm. Also, to achieve the optimum structure, the number of dielectric-like graphene layers is optimized to be 4. According to the abovementioned abbreviations, we

10.57647/ijbbe.2025.0502.10

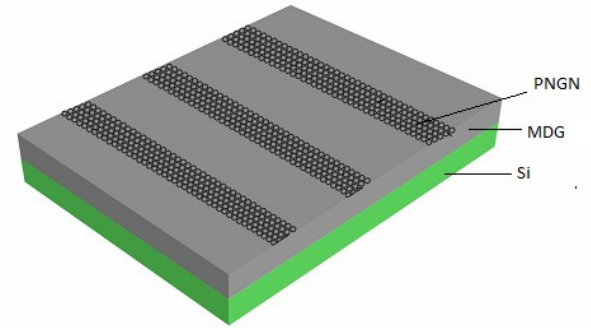

Figure 2. The proposed PNGN/MDG/Si waveguide structure consisting of an array of plasmonic nonlinear GNR with a thickness of 0.34 nm, a width of 50 nm, and a 150 nm distance gap. GNRs are deposited on a stack of the multi-layer dielectric- like-graphene where, a Si layer is considered as substrate

introduce our structure as PNGN/MDG/Si waveguide. Excitation of SPP at the interface of PNGN/MDG results in establishment of confined local electric fields. At the frequency of SPR, the plasmonic electromagnetic waves propagate perpendicular to these local fields and decay into the dielectric medium. This propagation leads to an enhancement of the electric field intensity within the dielectric medium. Based on Eq.9, the effective RI in the vicinity of GNR increases and establishes a local nonlinearity. This local nonlinearity results in a strong light confinement inside the waveguide where the reflectance profile tends to zero.

$$n_{eff} = \frac{c}{\omega}\int_0^{d_1} |E(x)|^2\, dx \qquad (9)$$

On the other hand, the PNGN medium significantly modifies the SPP wave vector because this vector is very sensitive to the RI of the medium. So, the optical response of the waveguide is affected by the nonlinearity of the PNGN medium. At the results section, we will show that the reflectance modification results in a nonzero profile where two symmetric peaks appear. While, for biosensor application we need to establish an asymmetric Fano profile, we embed an array of the graphene quantum dots (GQDs) at the top of waveguide. The GQD can be considered as a plasmonic nanoparticle that scatters light at the plasmonic resonance wavelength in different directions. So, the reflectance characteristics of the waveguide will be under the influence of the scattering direction. In this study, we exploit the GQDs with a diameter of 66 nm. The manufacturing process of this quantum dot was reported by pioneer researchers [37]. The permittivity of the mentioned GQD is obtained based on the Cole-Cole model through Eq. 10.

$$\varepsilon_{GQD=\varepsilon_\infty} + (\varepsilon_s - \varepsilon_\infty)/(1+(j\omega\tau)^{1-D}) \qquad (10)$$

where is the complex dielectric constant of the GQD, ε_∞ is the value of the dielectric constant at infinity, and is equal to 2.4. ε_s is the static dielectric constant, ω is the angular frequency, τ is the mean relaxation time, and is equal to 0.1195.D is the degree of the distribution time which, varies from 0 to 1. For our design and simulation at 380 °K, we consider D to be 0.2. $(\varepsilon_s - \varepsilon_\infty)$ is called dielectric strength and its value is equal to 4.69×10^{-9} [40]. Figure 3 demonstrates the proposed plasmonic nonlinear waveguide with GQDs on its surface. GQDs are separated by a distance of 100 nm from each other.

4. Results

We manipulate our simulation based on the reflectance profile of the waveguide. The reflectance characteristic of a structure is defined as R(ω) = 1 − A(ω) − T(ω). R(ω), A(ω), and T(ω) are the frequency dependent reflection, absorption, and transmission, respectively [41]. To extract the reflectance profile, we put the waveguide structure under the radiation of a light pump with TM polarization at the wavelength range of 1000 ~ 2000 nm, applying the FDTD method. We use the "power and field monitors" at the top and bottom of the structure. The FDTD simulator utilizes the Poynting theory to solve Maxwell equations to calculate the waveguide absorption through:

$$P_{abs} = -0.5\omega|E|^2 img(\varepsilon) \qquad (11)$$

where ω, |E|, and img (ε) are angular frequency, the intensity of the electric field, and the imaginary part of the permittivity, respectively [42, 43]. Figure 4 depicts the Normalized reflectance profile of PNGN/MDG/Si. We stack a 6-layer dielectric-like graphene to form MDG. Because, the optical and electrical properties of the multi-layer garaphen with more than 6 layers tend to the eproperties of bulk graphite [44].

At the wavelength of 1450 nm, where the frequency of the electromagnetic wave is the same as the oscillation frequency of the resonator free electrons, SPR occurs. SPR provides a strong concentration of the localized electric fields as shown in Figure 6(a). As a result, the reflectance profile at the SPP wavelength range of 1400 nm ~ 1500 nm becomes zero. But, the nonlinearity of the PNGN medium modifies the reflectance profile, resulting in two symmetric peaks located at the wavelengths of 1100 nm and 1650 nm. Figure 5 demonstrates the normalized reflectance profile of GQD/PNGN/MDG/Si waveguide. The light scattering by GQD affects the optical behavior of the proposed waveguide.

The GQDs perform as plasmonic nanoparticles in which their polarizability enhances the intensity of the electromagnetic field in their vicinity and distributes the concentration electric field at the PNGN/MDG structure, as shown in Figure 6(b). So, a sharp asymmetric peak is formed at the wavelength of 1100 nm.

The coupling between the broad resonance supported by SPP and the narrow resonance supported by the scattering effect leads to a sharp Fano resonance located at the wavelength of 1100 nm. The Fano resonance is highly sensitive to changes in the surrounding environment. Small perturbations in the medium can lead to significant shifts in the resonance position, width, and amplitude. This high sensitivity makes Fano resonances ideal for a variety of sensing applications, particularly in detecting minute changes in biological or chemical environments [8]. So, we design a biosensor based on the proposed waveguide. Figure 7 demonstrates the two-dimensional schematic of the proposed biosensor where a 10 nm air gap is abandoned between two symmetrical parts of biosensor. Each part consists of an array of PNGN with a thickness of 0.34 nm, and a width of 50 nm, in which the GQD's are located at a distance of 75 nm from the center of PNGN. A stack of 6 layers of MDG with a thickness of 6 nm, a Si layer with a thickness of 50 nm, and an Au layer with a thickness of 100 nm are the successive layers.

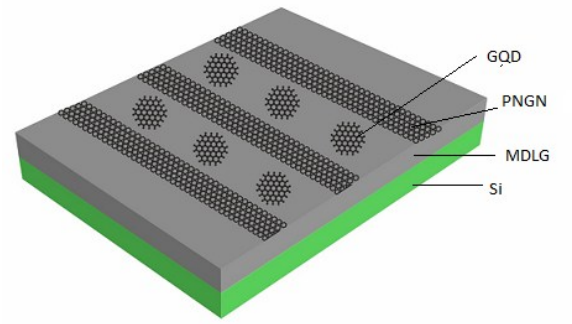

Figure 3. The proposed PNGN/MDG/Si waveguide structure with the GQDs. There is a 75 nm gap between GQDs and the GNRs

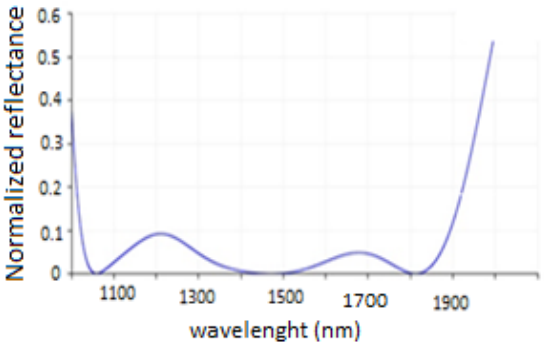

Figure 4. Normalized reflectance profile of PNGN/MDG/Si with two symmetric peaks at 1100 nm and 1560 nm

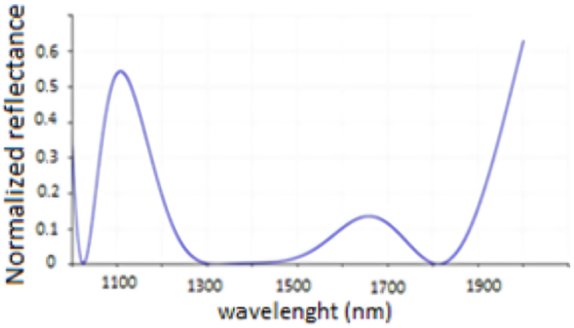

Figure 5. Normalized reflectance profile of GQD/PNGN/MDG/Si with a Fano resonance at 1100 nm

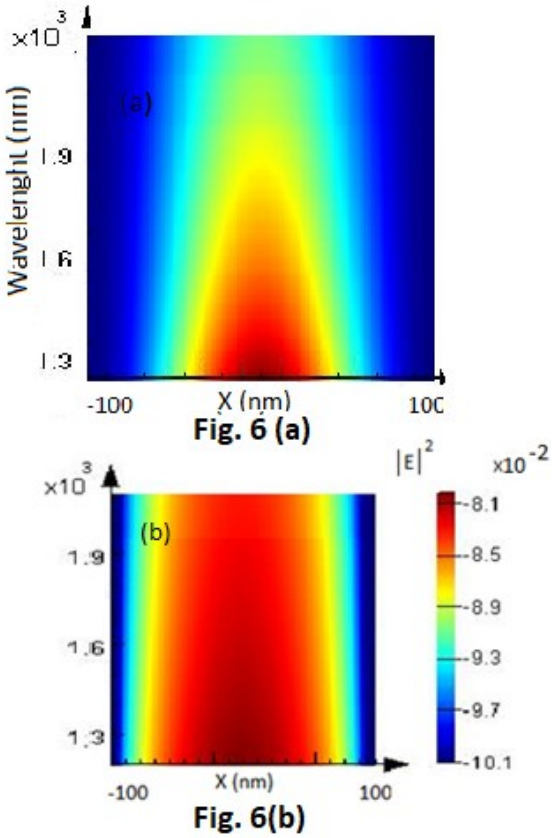

Figure 6. The distribution of the electric field in (a): the PNGN/MDG/ with concentrated field at the wavelength range of 1300~1500 nm, (b): GQD/PNGN/MDG with distributed field

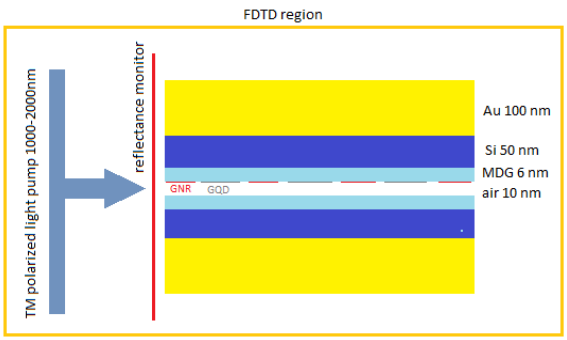

Figure 7. the proposed bio-sensor and a schematic of its simulation through FDTD method

The simulation was performed by replacing the air gap with a biomaterial medium having a RI of n=1.35. The RI of n=1.35 mimics the typical RI range of biological media, such as aqueous solutions containing proteins (e.g., bovine serum albumin, RI ≈ 1.33–1.36) or DNA strands (RI ≈ 1.34–1.37) [45]. We put the proposed biosensor structure under the radiation of a light pump with TE polarization at the wavelength range of 1000 ~ 2000 nm along X direction. The PML boundary condition is chosen along the X direction, and periodic boundary conditions are chosen along the Y and the Z directions. Two "power and field monitors" are used in the coordinates of -210 nm and +210 nm along the X direction as reflectance and transmittance monitors. Auto non-uniform mesh type with the accuracy of 6 and 0.25 nm mesh step is chosen as mesh settings where the length of the structure along the X direction is 400 nm. Dielectric volume average is applied as mesh refinement. Figure 8 shows the change in the Fano resonance wavelength as a function of the RI.

Simulation results reveal that replacing the air gap with a biomaterial medium having a RI of n=1.35, the Fano resonance wavelength shifts from 1120 nm to 1285 nm. An important criterion for evaluating sensors is the sensitivity (S), which is defined as the ratio of the wavelength shift (Δλ) of the Fano resonance spectrum to the change in the refractive index (Δn) as $S = \Delta\lambda/\Delta n\ (nm/RIU)$. In addition, the figure of merit (FOM) is another important indicator reflecting sensor performance, expressed as: $FOM = S/FWHM$. Where, FWHM represents the full width at half maximum of the resonance [9, 46]. Tab. 1 compares the characteristics of the proposed biosensor with similar studies.

The results demonstrate that the proposed structure still has some room for improvement. For the future plans, the characteristics improvement would be investigated based on the Fermi level of GNR.

This biosensor can be applied to detect the neurodegenerative disorders (NDDs) including, Parkinson's disease and Alzheimer's diseases where distinct proteins are considered to be involved. It should be noted that the detection of protein in the affected brain regions is a conventional medical method for diagnosing NDDs. NDDs are a set of heterogeneous disorders characterized by the progressive structural and functional degradation of the nerve cells and accumulation of misfolded and aggregated proteins in the affected brain regions [10]. Although most NDDs start 10 to 15 years before the manifestation of the clinical diagnostic symptoms, we still lack a reliable diagnostic method for early detection or monitoring of disease progression, thus precluding any effort for early intervention. Furthermore, NDDs are often misdiagnosed because of their clinical heterogeneity and overlapping symptoms.

Table 1. The comparison of the proposed biosensor characteristics with Fano-based SPP biosensors

biosensor	S(nm/RIU)	FOM	
G/CaF/Ge	461	-	[19]
Prism/metal/Silica	-	44	[47]
MIM	600	-	[46]
Proposed	471	43	

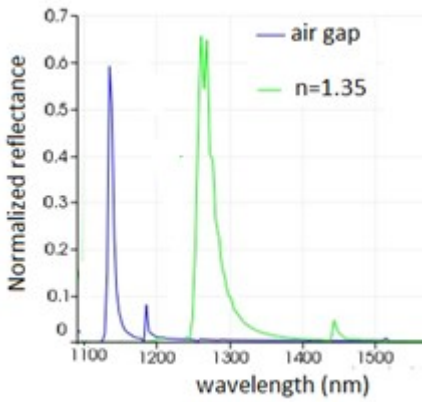

Figure 8. The change in Fano resonance wavelength due to the change in RI

For future research, the proposed biosensor can be combined with an AI algorithm based on the neural network (NN), where the output of the biosensor will be the input of the NN. These types of technologies introduce a platform for widespread clinical application for early detection of NDDs.

5. Conclusion

In this study, we designed an optical plasmonic waveguide based on plasmonic nonlinear GNR (PNGN) and a multi-layer dielectric-like graphene (MDG). Excitation of SPP at the interface of PNGN/MDG results in a Kerr-effect-like medium where the nonlinearity modifies the reflectance characteristic of the structure. The electric field concentration and light confinement establish a broad resonance mode at the wavelength of 1400 nm~1500 nm. Then we embedded an array of the quantum dots (GQDs) between PNGNs. Due to the scattering effect of GQDs, the near-filed-enhancement effect occurs in the vicinity of GQDs, resulting in the distribution of the electric field, and the establishment of the narrow resonance mode. The coupling between the broad and narrow resonance modes creates a Fano resonance that is highly sensitive to the RI of the surrounding media. Changing the RI to the RI of the biomedical media results in a significant change in the Fano resonance position. These findings prove that the GQD/PNGN/MDG structure can be applied to the

detection of RI-induced characteristics as a biosensor. Then, we designed a biosensor based on our waveguide where a narrow air gap is abandoned between its parts. Replacing the air gap with the biomaterial medium having the RI of n=1.35 shifts the Fano resonance wavelength. This finding proves the designed biosensor ability in detection of neurodegenerative disorders. The sensitivity and FOM of the designed biosensor were computed as 471 nm/RIU and 43, respectively.

Authors Contribution
All authors have contributed equally to prepare the paper.

Availability of data and materials
The data that support the findings of this study are available from the corresponding author, upon reasonable request.

Conflict of interests
The authors declare that they have no known competing financial interests or personal relationships that could have appeared to influence the work reported in this paper.

References

[1] Haji Najafi, M.J., Ahmadi, V., Hamidi, S.M., Design and Analysis of Graphene Based SPR Biosensor Using Ellipsometry Method. in Iranian nano photonic conference. 2020: Sistan University, Iran.

[2] Mehrpanah, A., et al., (2024). Absorption Enhancement of Thin Film Solar Cell Utilizing a Graphene-Based Metasurface. Journal of Optoelectronical Nanostructures, 9(4).
DOI: https://doi.org/10.71577/jopn.2024.1182795

[3] Mehrpanah, A., et al., (2024). Design of Graphene-Based Core/Shell Nanoparticles to Enhance the Absorption of Thin Film Solar Cells. Plasmonics,
DOI: https://doi.org/10.1007/s11468-024-02476-1

[4] Kim, J.T., & Choi, S.-Y. (2011). Graphene-based plasmonic waveguides for photonic integrated circuits. Optics Express, 19(24), 24557-24562
DOI: https://doi.org/10.1364/OE.19.024557

[5] Schröder, B. (2020). Probing Light-Matter Interactions in Plasmonic Nanotips. Dissertation, Göttingen, Georg-August Universität, 2020.

[6] Sharma, T., et al., (2024). Past, present, and future of hybrid plasmonic waveguides for photonics integrated circuits. Nanotechnology and Precision Engineering, 7(4).
DOI: https://doi.org/10.1063/10.0028127

[7] Selvaraja, S.K. & Sethi, P. (2018). Review on optical waveguides. Emerging Waveguide Technology, 95, 458.
DOI: https://doi.org/10.5772/intechopen.77150

[8] Sharifi, M., Tajalli, H., & Pourasl, M. (2024). Design of Metal-Insulate-Metal Plasmonic Waveguide Biosensor for Disease Diagnosis. International Journal of Biophotonics and Biomedical Engineering (IJBBE), 4(2), 23-30.
DOI: https://doi.org/10.71498/ijbbe.2024.1191244

[9] Zhu, J. & Wu, C. (2021). Optical refractive index sensor with Fano resonance based on original MIM waveguide structure. Results in Physics, 21, 103858.
DOI: https://doi.org/10.1016/j.rinp.2021.103858

[10] Kavungal, D., et al., (2023). Artificial intelligence–coupled plasmonic infrared sensor for detection of structural protein biomarkers in neurodegenerative diseases. Science Advances, 9(28), eadg9644.
DOI: https://doi.org/10.1126/sciadv.adg964

[11] Li, Z., Zhang, W., & Xing, F. (2019). Graphene optical biosensors. International journal of molecular sciences, 20(10), 2461.
DOI: https://doi.org/10.3390/ijms20102461

[12] Li, J., et al., (2016). All-optical controlling based on nonlinear graphene plasmonic waveguides. Optics express, 24(19), 22169-22176.
DOI: https://doi.org/10.1364/OE.24.022169

[13] Sarkhoush, M., Rasooli Saghai, H., & Soofi, H. (2022). Design and simulation of type-I graphene/Si quantum dot superlattice for intermediate-band solar cell applications. Frontiers of Optoelectronics, 15(1), 42.
DOI: https://doi.org/10.1007/s12200-022-00043-2

[14] Song, B., et al., (2010). Graphene on Au (111): a highly conductive material with excellent adsorption properties for high-resolution bio/nanodetection and identification. ChemPhysChem, 11(3), 585-589.
DOI: https://doi.org/10.1002/cphc.200900743

[15] Wu, L., et al., (2010). Highly sensitive graphene biosensors based on surface plasmon resonance. Optics express, 18(14), 14395-14400.
DOI: https://doi.org/10.1364/OE.18.014395

[16] Salihoglu, O., Balci, S., & Kocabas, C. (2012). Plasmon-polaritons on graphene-metal surface and their use in biosensors. Applied Physics Letters, 100(21).
DOI: https://doi.org/10.1063/1.4721453

[17] Ruan, B., et al., (2017). Ultrasensitive terahertz biosensors based on Fano resonance of a graphene/waveguide hybrid structure. Sensors, 17(8), 1924.
DOI: https://doi.org/10.3390/s17081924

[18] Salehnezhad, Z., Soroosh, M., & Farmani, A. (2023). Design and numerical simulation of a sensitive plasmonic-based nanosensor utilizing MoS2 monolayer and graphene. Diamond and Related Materials, 131, 109594.
DOI: https://doi.org/10.1016/j.diamond.2022.109594

[19] Dai, X., Ruan, B., & Xiang, Y. (2021). Self-referenced refractive index biosensing with graphene Fano resonance modes. Biosensors, 11(10), 400.
DOI: https://doi.org/10.3390/bios11100400

[20] Li, Y., et al., (2022). Graphene metasurfaces for terahertz wavefront shaping and light emission. Optical Materials Express, 12(12), 4528-4546.
DOI: https://doi.org/10.1364/OME.473110

[21] Mehrpanah, A., et al., (2024). Absorption Enhancement of Thin Film Solar Cell Utilizing a Graphene-Based Metasurface. Journal of Optoelectronical Nanostructures, 35(4),
DOI: https://doi.org/10.71577/jopn.2024.1182795

[22] Jiang, X., Yuan, H., & Sun, X. (2016). Nonlinear plasmonic dispersion and coupling analysis in the symmetric graphene sheets waveguide. Scientific Reports, 6(1), 39309.
DOI: https://doi.org/10.1038/srep39309

[23] He, X.Y. & Li, R. (2013). Comparison of graphene-based transverse magnetic and electric surface plasmon modes. IEEE Journal of Selected Topics in Quantum Electronics, 20(1), 62-67.
DOI: https://doi.org/10.1109/JSTQE.2013.2257991

[24] Kauranen, M. & Zayats, A.V. (2012). Nonlinear plasmonics. Nature photonics, 6(11), 737-748.
DOI: https://doi.org/10.1038/nphoton.2012.244

[25] Newell, A. Nonlinear optics. (2018). CRC Press.
DOI: https://doi.org/10.1201/9780429502842

[26] Shi, Z., et al., (2016). Broadband tunability of surface plasmon resonance in graphene-coating silica nanoparticles. Chinese Physics B,
DOI: https://doi.org/10.1088/1674-1056/25/5/057803

[27] Kanani, H., et al., (2024). Design of Graphene-Coated Silver Nanoparticle Based on Numerical Solution to Enhance the Absorption of the Thin-Film Solar Cell. Plasmonics, 1-9.
DOI: https://doi.org/10.1007/s11468-024-02231-6

[28] Zhang, Y., et al., (2023). Plasmonic characteristics of the graphene-photonic crystal composite structure in the IR regime. Plasmonics, 18(1), 125-135.
DOI: https://doi.org/10.21203/rs.3.rs-1664963/v1

[29] Liu, J.-X., et al., (2020). A research of Drude-two-critical points model of graphene near the optical frequency. Superlattices and Microstructures, 148, 106692.
DOI: https://doi.org/10.1016/j.spmi.2020.106692

[30] Figueiredo, J.L., Bizarro, J.P., & Terças, H. (2022). Weyl–Wigner description of massless Dirac plasmas: ab initio quantum plasmonics for monolayer graphene. New Journal of Physics, 24(2), 023026.
DOI: https://doi.org/10.1088/1367-2630/ac5132

[31] Liu, Y.-Q., Li, L. & Yin, H.(2018). Studies on Surface Plasmon Dispersion Theory on the Bilayer Graphene Ribbon Arrays Metasurface. in IEEE International Conference on Computational Electromagnetics (ICCEM). IEEE.
DOI: https://doi.org/10.1109/COMPEM.2018.8496505

[32] Slizovskiy, S., et al., (2021). Out-of-plane dielectric susceptibility of graphene in twistronic and bernal bilayers. Nano Letters, 21(15), 6678-6683.
DOI: https://doi.org/10.1021/acs.nanolett.1c02211

[33] Raad, S.H. & Atlasbaf, Z. (2021). Solar cell design using graphene-based hollow nano-pillars. Scientific Reports, 11(1), 16169.
DOI: https://doi.org/10.1038/s41598-021-95684-2

[34] Sarkhoush, M., Rasooli Saghai, H., & Soofi, H. (2023). Type-I graphene/Si quantum dot superlattice for intermediate band applications. Journal of Solar Energy Research, 8(1), 1317-1325.
DOI: https://doi.org/10.22059/jser.2022.349258.1257

[35] Chorsi, H.T. & Gedney, S.D. (2016). Tunable plasmonic optoelectronic devices based on graphene metasurfaces. IEEE Photonics Technology Letters, 29(2), 228-230.
DOI: https://doi.org/10.1109/LPT.2016.2636813

[36] Dave, V., et al., (2018). Graphene based tunable broadband far-infrared absorber. Superlattices and Microstructures, 124, 113-120.
DOI: https://doi.org/10.106/j.spmi.2018.10.013

[37] Sikdar, D. & Premaratne, M. (2014) Electrically tunable directional spp propagation in gold-nanoparticle-assisted graphene nanoribbons. in IEEE Photonics Conference.
DOI: https://doi.org/10.1109/IPCon.2014.6995378

[38] Wang, D., et al. (2015). Plasmon resonance in single-and double-layer CVD graphene nanoribbons. in Conference on Lasers and Electro-Optics (CLEO). IEEE.
DOI: https://doi.org/10.1364/CLEO_QELS.2015.FTu1E.3

[39] Cao, S., et al., (2018). Graphene–silver hybrid metamaterial for tunable and high absorption at mid-infrared waveband. IEEE Photonics Technology Letters, 30(5), 475-478.
DOI: https://doi.org/10.1109/LPT.2018.2800729

[40] Tripathi, H.S., et al. (2019). Insulator to semiconductor transition in graphene quantum dots. in AIP Conference Proceedings. AIP Publishing.
DOI: https://doi.org/10.48550/arXiv.1905.04047

[41] Hossain, M.J., Faruque, M.R.I., & Islam, M.T. (2019). Perfect metamaterial absorber with high fractional bandwidth for solar energy harvesting (vol 13, e0207314, 2018). PLOS ONE, 14(1).
DOI: https://doi.org/10.1371/journal.pone.0207314

[42] Tharwat, M.M., Almalki, A., & Mahros, A.M. (2021). Plasmon-enhanced sunlight harvesting in thin-film solar cell by randomly distributed nanoparticle array. Materials, 14(6), 1380.
DOI: https://doi.org/10.3390/ma14061380

[43] Heidarzadeh, H., Jangjoy, A., & Bahador, H. (2022). Use of coupled Al-Ag bimetallic cylindrical nanoparticles to improve the photocurrent of a thin-film silicon solar cell. Plasmonics, 17(3), 1323-1329.
DOI: https://doi.org/10.1007/s11468-022-01630-x

[44] Arefinia, Z., & Asgari, A. (2017). Optimization study of a novel few-layer graphene/silicon quantum dots/silicon heterojunction solar cell through opto-electrical modeling. IEEE Journal of Quantum Electronics, 54(1), 1-6.
DOI: https://doi.org/10.1109/JQE.2017.2774144

[45] Sekhwama, M., et al. (2024). Enhancing limit of detection in surface plasmon resonance biosensors: A sensitivity analysis for optimal performance. in Optical Interactions with Tissue and Cells XXXV. SPIE.
DOI: https://doi.org/10.1117/12.3002449

[46] Meng, Q.-Q., et al. (2017). Figure of merit enhancement of a surface plasmon resonance sensor using a low-refractive-index porous silica film. Sensors, 17(8), 1846.
DOI: https://doi.org/10.3390/s17081846

[47] Li, S., et al. (2016). Tunable triple Fano resonances based on multimode interference in coupled plasmonic resonator system. Optics Express, 24(14), 15351-15361.
DOI: https://doi.org/10.1364/OE.24.015351